

SAR IMAGE GEOCODING USING A STEREO-SAR DEM AND AUTOMATICALLY GENERATED GCPs

Pu-Huai CHEN, Ian DOWMAN,
University College London, U.K.
Department of Geomatic Engineering
idowman@ge.ucl.ac.uk

KEY WORDS: Automation, Control strategies, DEM, Geo-referencing, RADARSAT, Simulation, Spatial data, Stereo SAR.

ABSTRACT

SAR image geocoding needs an accurate DEM, but such a DEM can be difficult to obtain. This paper shows that the needs of geocoding can be satisfied using the DEM generated by employing a rigorous geometric model and an optimized least squares correlation method with a region-growing approach. The geometric model used is independent of any manually selected GCPs and is robust to orbit errors. The required number of GCPs for correcting any systematic effects after space intersection is only two. When good quality orbit information is unavailable, GCPs or tie points are essential for SAR image geocoding, but selection and measurement of these points is often difficult.

This paper proposes a SAR simulation technique to automatically provide control for geocoding without manually selected GCPs or tie points. The GCPs were generated using a small known DEM chip of size 1km by 1km with significant terrain relief. The RMS errors of the four automatically generated GCPs are less than 3.4m in range direction and 4.6m in azimuth direction. RADARSAT SAR images have been tested using a reference DEM and an automatically generated DEM to produce geocoded images. The RMS errors of the check points range from 13m to 21m in easting and 16m to 21 in northing. The results derived in this paper demonstrate that the stereo-SAR generated DEM can be used for geocoding in flat-moderate areas, and a higher level of automation can be achieved.

1 INTRODUCTION

Geocoding is to geometrically rectify a remotely sensed image, such as a Synthetic Aperture Radar (SAR) image, according to a specific map projection and a Digital Elevation Model (DEM) to eliminate terrain induced image distortions. The key factor to produce a geocoded radar image-map is the use of a correct DEM and reliable Ground Control Points (GCPs). However, DEMs are not always available and may be difficult to produce, e.g. in cloud-covered locations where optical data is not available or in underdeveloped areas where collecting GCPs is difficult. Two distinctive and practical methods have been developed for generating a DEM from SAR data, including interferometric SAR (IfSAR) and stereoscopic SAR, (Leberl, 1990).

In terms of frequent mapping and global monitoring, however, experiments of the repeat-pass space-borne IfSAR system show that the method often gives poor results due to poor coherence and to different atmospheric and physical conditions. Compared with IfSAR approach, the stereoscopic SAR method, based on measuring the co-ordinate difference of a common ground point from an image pair and converting it to spatial data according to an appropriate geometric model, does not require such tight conditions. Another advantage of the stereoscopic SAR method is the ability of direct provision of the spatial information of any image point and of linear/area measures. It means that the stereo SAR method is relatively flexible. In theory, there also remain other conditions for stereo SAR, such as a reasonable intersection angle between each image for collecting distinctive parallaxes, allowing them to be transformed into height data. This condition is less significant, since multiple options of incidence angle of space-borne SAR data are available nowadays, such as RADARSAT data, (CSA, 1995). The Shuttle Radar Topography Mission (SRTM) was launched in early 2000, it uses a single-pass IfSAR system and is designed to carry out terrain elevation mapping of 80% of the Earth's land surface, (JPL, 2000). It will be shown later that the stereoscopic radargrammetric method can be used as an alternative tool for general mapping to the IfSAR approach, whenever the IfSAR method is not applicable or the IfSAR generated DEM is not available to common users.

A rigorous geometric algorithm for generating spatial information with an error model to be validated is necessary to understand the full potential and limitations of extracting spatial information from stereoscopic SAR data. Also, the requirements of human operations and GCPs have to be reduced. Early work on ERS-1 data at UCL suggests that the stereoscopic radargrammetric approach is a promising tool for extracting elevation data from space-borne SAR data,

(Clark, 1991). Chen and Dowman (1996) proposed an analytic approach to carry out space intersection using the least-squares adjustment for ERS-1 data and reported results without using any GCPs, if good quality orbit data is available. Further consideration and refinement for the geometric model to be applied to the SAR data with inferior quality orbit data, such as RADARSAT SAR imagery, has been carried out (Chen, 2000). Image correlation is one of the key steps from analytic to digital radargrammetry. Pyramidal correlation strategy using the least-squares correlation method with a region-growing approach has been proved useful to generate a parallax file from SIR-B SAR data, (Denos, 1992), and a DEM can be generated from ERS-1 images (Twu, 1996). An optimized strategy for giving the pyramidal structure has also been developed (Dowman and Chen, 1998).

Providing ground control is indeed a problem in digital radargrammetry. Manual operations for collecting GCPs from radar images and maps are usually limited by visual image-map correlation, and are not always stable hence the GCP quality cannot be assured. In order to cope with this problem, SAR image simulation techniques have been used for provision of ground control in geocoding, for instance, Kwok *et al.* (1990) and Guindon (1995). The accuracy of the automatically provided ground control relies on the quality of the simulator as well as on the outcome derived from the real-simulated SAR image correlation. Poor quality simulated images may lead to poor results of real-simulated image correlation. Previous work shows that most of the currently available SAR image simulators still require many human interventions. A SAR image simulator is designed to provide ground control by using four corner elements of a known DEM chip, according to a SAR imaging model to relate the DEM sensed and the SAR image, provided that a small DEM chip with significant terrain relief is available (Chen, 2000).

This paper describes the use of the DEMs derived from stereo RADARSAT SAR data and the automatically derived GCPs for geocoding to achieve a higher level of automation in radargrammetry. Section 2 reviews the algorithms developed briefly. The detailed descriptions of the algorithms proposed in this paper are given in Chen (2000). In section 3, the accuracy of the DEM derived and the GCPs generated automatically are verified. The geocoded SAR images derived, as shown in section 4, are used to verify the proposed algorithms.

2 ALGORITHMS

2.1 Automatic Generation of DEMs from Stereo SAR Data

Generation of spatial data from a pair of stereo SAR images requires a geometric model and an image correlation method. An ideal geometric model for extracting spatial data from a SAR image pair is expected to obtain high quality results, to require a minimal number of GCPs and human interventions. The range/Doppler equations can be used as observation equations in a least squares adjustment for solving ground points from ERS data, (Chen and Dowman, 1996). Refinement of the algorithm has been made using a weighting matrix to cope with inferior orbit data provided by RADARSAT SAR imagery in order that the effects from the azimuth timing error on the results derived can be minimized. GCPs are not required in the geometric model. Systematic correction can be made using only two GCPs after space intersection. An area-based least squares correlation method, (Gruen, 1995), with a region-growing approach, (Otto and Chau, 1989), is adopted to generate a dense coverage of elevation data set. This method has been refined using a pyramidal harness to propagate control from the top to bottom image tier hence the effect of speckle in SAR imagery can be reduced, (Denos, 1992). An optimized strategy of parameter determination for commanding the pyramidal structure has been proposed to improve the level of automation, provided that the maximal parallax of the image pair to be correlated can be measured or calculated using a coarse DEM, (Dowman and Chen, 1998).

2.2 Automatically Generated Control

In order to reduce manual operations, and then to stabilize the quality of GCPs, a SAR image product simulation method is proposed to automatically provide ground control for radargrammetry. The proposed simulator is based on the assumption of the perpendicular relationship between the resultant range and velocity vectors in SAR imagery. A known DEM chip of a small area with varied terrain surface and the header/orbit data of a real SAR image are required. Also, it is assumed that the structure of a real SAR image is well defined by the header/orbit information allowing automatic detection of the extent of the simulated area without human intervention. The geometric considerations for a SAR image simulator include the simulation of the image structure of a real image with no manually defined parameters required, such as the range and azimuth time offsets for a sub-scene SAR image and incidence angles for individual pixels. In terms of radiometry, a simple reflectivity model is applied to the entire simulated area without regard to speckle or different ground cover. The reflectivity model is defined as the scalar product of a range vector from the sensor to a DEM element and the outward surface normal of that DEM cell of interest. This simplification cannot be avoided because the detailed ground truth data of an arbitrary real image, which affects the reflectance of a radar wave, is not always available.

2.2.1 SAR Image Simulation. The track of a sensor in 3-D space is a smooth curve that is continuous and differentiable. There always exists a tangent passing through a point on the orbit and a normal plane perpendicular to the tangent at that point. Physically, the position vector of a SAR sensor is changing along its orbit corresponding to its azimuth time and the tangent at that point is equivalent to the sensor velocity vector. The normal plane passing through that point represents a zero-Doppler plane with an equal range circle from the sensor to ground points. The concept of the proposed SAR simulation method is based on the zero-Doppler imagery and on a scanning process from the first azimuth line to the last one through the entire simulated area for detecting any DEM element encountered. Each normal plane derived along the orbit track resembles the corresponding azimuth line of a simulated SAR image.

2.2.2 Real-Simulated Image Correlation. Four corner points of the known DEM chip are treated as GCPs whose ground co-ordinates are already known, but the real image co-ordinates of the GCPs have to be derived using a real-simulated image correlation technique. The well-known normalized cross-correlation measure is adopted to search for the best match of the corresponding position of the simulated image within the real image co-ordinate system. The simulator also records the simulated range and azimuth time data of the GCPs based on the SAR imaging geometry when the GCPs are detected in the process of simulation. The simulated range and azimuth time data of the GCPs can be compared with those observations of the real image that gives the range and azimuth timing shifts and can be used to provide control in geocoding.

2.3 Refinement of the DEM

Using the rigorous algorithm of space intersection and the pyramidal image correlation scheme with a region-growing technique directed by an optimized parameter selection strategy, a raw DEM composed of irregularly distributed ground points can be derived. Further effort for the automatic provision of ground control that improves the accuracy of the GCPs used, ensures the quality of the radargrammetric results derived. The DEM obtained is, however, incomplete in terms of practical applications, which demand spatial data without gaps or blunders. There are typical terrain induced effects in a SAR image pair, for example, layover, leading to the formation of gaps in a raw DEM generated. These effects decrease the quantity, and deteriorate the quality, of the results derived from image correlation routines. A method of data fusion for the DEMs generated can be made to improve the DEM coverage without degrading the overall accuracy, for example, filling the major gaps using the DEMs generated from different orbit directions. Since the original elevation data is not changed, there is no effect on the quality of the DEM derived, but the coverage of that DEM can be improved efficiently. Further improvements can be made using an interpolation method to fill minor gaps. This makes a 'complete' DEM without gaps or voids. In addition, a filtering technique is employed to suppress noise and to derive a practical DEM. Filtering DEMs can have a significant effect on the final results. A quality check for the DEM derived is essential for each step of refinement.

2.4 SAR Image Geocoding

Geocoded SAR images have been used as an application example of the stereo-generated DEM to validate the proposed algorithms. Thus, an algorithm with the minimal degradation of accuracy for the SAR image geocoding must be considered. Precise terrain corrected geocoding of SAR imagery requires a known DEM, the imaging geometry/orbit data and GCPs or tie points. Recent geocoding methods for ERS-1 data employ a map-to-image transformation based on the range-Doppler equations, for instance, Dowman *et al.* (1993). The range-Doppler approach is performed only for an anchor point grid (or a super-grid structure) constructed by regularly distributed DEM elements to reduce computational load. All of the other DEM elements are then transformed into image co-ordinates by an efficient bilinear interpolation (or other polynomial fit functions), according to the anchor point grid established. A direct approach relating the SAR image to object space has been developed that ensures the minimal accuracy degradation in geocoding. The proposed geocoding process resembles the principle of the proposed method of SAR image simulation. Since no polynomial fit functions are used, the risks of possible errors caused by the polynomial fit functions can be completely avoided. Absolute ground control for geocoding is usually provided using the manually collected GCPs whose quality is not always stable. In order to get rid of any human interventions for collecting GCPs, the automatically generated GCPs are used to correct the range and azimuth timing errors in the header/orbit files.

3 TEST DATA AND VERIFICATION OF THE DEM AND GCPS GENERATED

Under the RADARSAT Application Development and Research Opportunity (ADRO) Programme, four RADARSAT images provided by the RADARSAT International (RSI) have been tested for generation of DEMs and geocoded images. These images cover the Aix-Marseilles test area in South France with varied terrain utilization and spatial

characteristics. The variation of terrain surface ranges from 0m to 640m above mean sea level. The SAR images used in experiments are grouped into two pairs according to orbit direction, as listed in Table 1.

| Orbit direction | RADARSAT beam mode | Acquisition date | Full-scene size (row/column) | Sub-scene for image correlation (row/column) | Alias name |
|-----------------|--------------------|------------------|------------------------------|----------------------------------------------|------------|
| Descending pair | Standard-1 | 1997-08-22 | 7901 / 9075 | 1024 / 1024 | DS1 |
| | Standard-7 | 1998-03-13 | 7875 / 8937 | 1024 / 1024 | DS7b |
| Ascending pair | Standard-1 | 1998-03-01 | 7876 / 8961 | 1024 / 1024 | AS7 |
| | Standard-7 | 1997-08-08 | 7901 / 9139 | 1024 / 1024 | AS1 |

Table 1. Four SAR images being simulated.

Notice that the acquisition time of each image varies by more than six months! Using the rigorous algorithm of space intersection and the pyramidal image correlation scheme with a region-growing technique directed by an optimized parameter selection strategy, two raw DEMs were derived from the ascending and descending image pairs. Using straightforward data addition, two raw DEM data files can be merged together giving a new DEM with better coverage, but no quality degradation. The DEM generated was interpolated into a 12.5m grid and sectioned for the effective area of 10km × 10km, as shown in Figure 1. The interpolated DEM can be refined further using a moving average filter (radius=3 pixels) to suppress possible noise. The statistics of the accuracy of the DEM derived from each step of refinement, as shown in Table 2, were compared with a reference DEM of the test area, as shown in Figure 2.



Figure 1. The DEM generated and refined (10km × 10km)

The reference DEM is of size 13.5km × 13.5 km (271 × 271 pixels) in a 50m grid with accuracy of 5m in elevation and in the French Lambert Conformal Conic Zone III map projection system. In order to provide control in radargrammetry, two manually selected GCPs could be used to provide control. However, since a known DEM chip of size 1km × 1km (21 × 21 pixels) is available, as shown in Figure 2 (right), it was used for SAR image simulation to generate four GCPs automatically showing that the systematic shift in the raw DEMs can be eliminated as demonstrated in Table 2. As mentioned before, the simulated image based on the known DEM chip has to be correlated with the real image to provide control. Examples of the simulated image chips are shown in Figure 3 (right) with the correlated real counterpart as shown in Figure 3 (left). The size of each simulated image chip varies according to the radar illumination and direction of the real orbit track, as shown in Table 3.

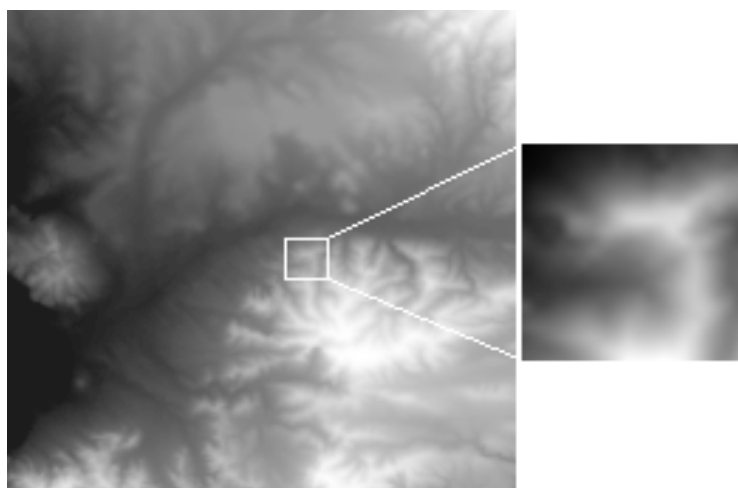


Figure 2. Left: reference DEM (IGN ©, size: 13.5km × 13.5km in a 50m grid,). Right: a DEM chip (1km × 1km) to be used in SAR image simulation for providing control.

| DEM Type | DEM Processing | GCPs | Mean (m) | RMS (m) | Min. (m) | Max. (m) |
|--------------|-----------------------------|-----------|---------------|--------------|-------------|-------------|
| Original DEM | (descending pair) | Manual | +1.4 | 23.9 | -189 | +223 |
| | (descending pair) | Automatic | +1.4 | 23.9 | -189 | +223 |
| | (ascending Pair) | Manual | 10.2 | 23.4 | -209 | 233 |
| | (ascending Pair) | Automatic | +2.3 | 23.6 | -217 | +219 |
| Refined DEM | Data addition | Automatic | +1.8 | 23.8 | -217 | +223 |
| | Interpolation | Automatic | -1.595 | 21.63 | -192 | +138 |
| | Filtering (radius=3) | Automatic | -1.596 | 20.74 | -170 | +132 |

Table 2. Statistics of the generated DEMs.

The calculated range and azimuth time of the four GCPs generated automatically were compared with the observations of the real SAR images giving range and azimuth time shifts as shown in Table 4. It can be seen that there are significant shifts (mean values in Table 3) in the orbit data, which differ from -41m to +110m in range and -151m to +61m in azimuth direction in

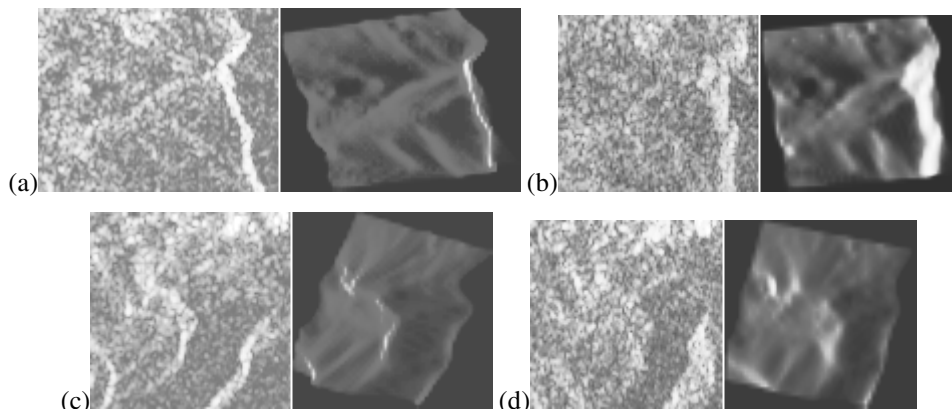


Figure 3 Real (left)-simulated (right) image chips. (a) DS1 (93 × 121 pixels). (b) DS7b (89 × 100 pixels). (c) AS1 (95 × 96 pixels). (d) AS7 (98 × 101 pixels)

terms of the product of the averaged sensor speed (7500m/sec) and the azimuth time shift. Also, it is obvious that the RMS error of individual GCPs derived automatically is less than 0.4 pixel of a RADARSAT standard image. The range and timing shifts will be considered and imported to the geocoding routine to correct orbit data errors.

| Alias name | DS1 | DS7b | AS1 | AS7 |
|-----------------------------------|----------|----------|---------|----------|
| Simulated image size (row/column) | 93 / 121 | 89 / 100 | 95 / 96 | 98 / 101 |

Table 3. Statistics of the four automatically generated GCPs.

| Alias name | | DS1 | DS7b | AS1 | AS7 |
|---------------------------|------------|--------------|--------------|--------------|--------------|
| Range Difference | Mean (m) | +94.2 | -41.4 | +8.3 | +110.0 |
| | RMSE (m) | 2.6 | 2.2 | 1.6 | 3.4 |
| Azimuth Timing Difference | Mean (sec) | -0.00617 | -0.02023 | +0.01412 | +0.00825 |
| | (m) | (-46.0) | (-150.7) | (+105.2) | (+61.5) |
| | RMSE (sec) | 0.00027 | 0.00008 | 0.00062 | 0.00017 |
| | (m) | (2.0) | (0.6) | (4.6) | (1.3) |

Table 4. Statistics of the four automatically generated GCPs.

4 TEST OF GEOCODING

4.1 Geocoding Using the Reference DEM

An example of the geocoded images (DS1) derived using the reference DEM is shown in Figure 4. The reference DEM has to be interpolated into a 12.5m grid to cope with the pixel spacing of the geocoded image required. Seven check points were selected from the test area to evaluate the accuracy of the geocoded image derived. Due to the difficulty in identification of the image features in SAR images, all of the check points measured are the corners of buildings. The elevation of each object measured is not known.

The co-ordinates in plan of each check point measured from the geocoded image and from a 1:25,000 scale map were compared, giving statistics in respect to each geocoded image as in Table 4 and showing that the RMS errors are below 21m in easting (E) or northing (N). Notice that the nominal resolution of a RADARSAT standard image is 25m. In addition, the elevation of each object measured, which is liable to cause layover effect and local displacement in plan, has not been corrected. The deviations derived show the resultant accuracy of the reference DEM, the performance of the geocoding algorithm and the measuring error of a human operator. The

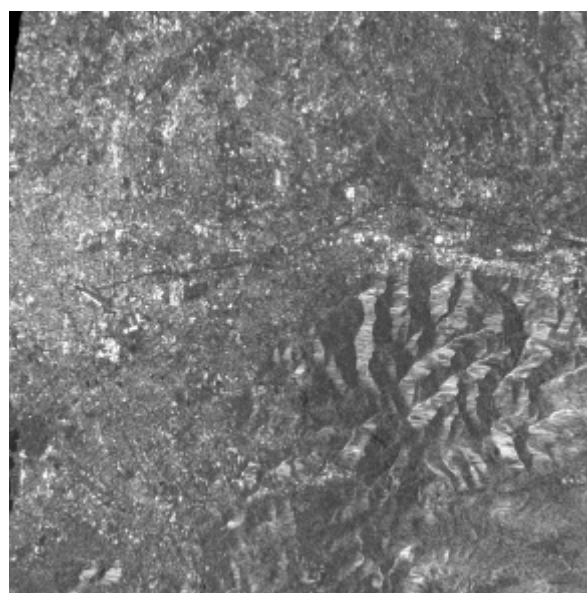


Figure 4. Geocoded image DS1 derived using the reference DEM (11km × 11 km)

deviations in E or N of check points calculated and averaged from four geocoded images are also shown in Figure 5 to demonstrate the error behavior. Generally speaking, there is no significant systematic shifts being shown. It proves that the automatically generated GCPs do work reasonably. However, the elevation of each object measured is strongly related to layover effect as can be seen from the difference of mean values shown in Table 4, particularly in the cases of high-incidence-angle images, such as DS1 and AS1. Also, the human operator's error cannot be underestimated due to the difficulty in the process of manual map-image correlation. Tests of geocoding for the DEM generated and refined are given in next section.

| Alias Name | DS1 | | DS7b | | AS1 | | AS7 | | Mean (m) | |
|------------|-----|----|------|----|-----|----|-----|----|----------|----|
| Component | E | N | E | N | E | N | E | N | E | N |
| Mean (m) | -32 | +1 | +15 | +3 | -19 | +9 | +2 | +2 | -8 | +3 |
| RMSE (m) | 21 | 16 | 13 | 21 | 21 | 18 | 18 | 19 | | |
| 2-D (m) | 26 | | 25 | | 28 | | 26 | | | |

Table 4. Positioning accuracy of the check points measured in respect to each geocoded image derived using the reference DEM.

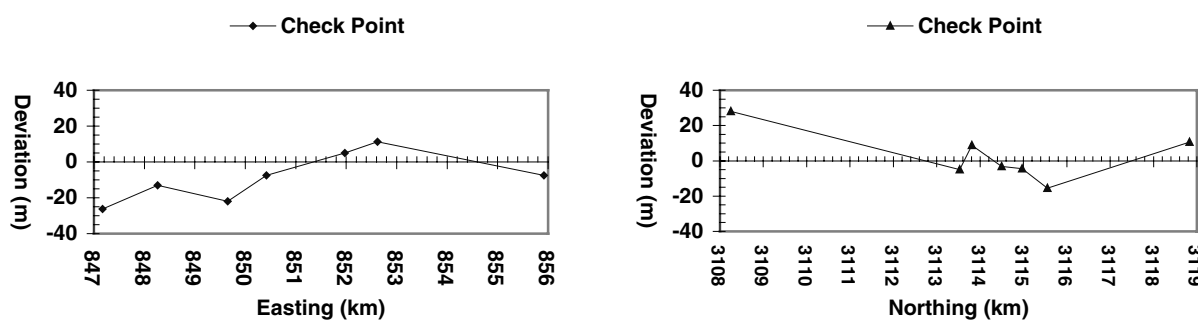


Figure 5. Deviations of the check points (in easting, left, and in northing, right) measured and averaged from the four geocoded images derived using the reference DEM.

4.2 Geocoding Using the Derived and Refined DEM

Based on the same ground control as described in Section 4.1, and the RADARSAT SAR orbit data, geocoded images were generated using the derived and refined DEM, as shown in Figure 6. In terms of visual comparison between Figure 4 and 6, the differences of both images are concentrated in the hilly areas (the central and southeastern part of the test area). This is because information extraction in hilly areas, where layover effect is significant, is incomplete, hence the DEM derived in hilly areas is relatively less reliable.

The same seven check points were selected from the test area to evaluate the accuracy of the geocoded image derived using the generated and refined DEM. The coordinates in plan of each check point measured from the geocoded image and from a 1:25,000 scale map were compared giving statistics in respect to each geocoded image as in Table 5 showing that the RMS errors are below 24m in easting (E) or northing (N). Table 4 and 5 shows similar RMS error magnitudes in E or N. The mean values of positional errors in terms of the geocoded images derived using the generated DEM, as shown in Table 5, are slightly better than those of the geocoded images derived using the reference DEM. It is probably because the reference DEM gives elevation at the ground level, but the generated DEM is referred to the 'rooftop' level (of ground cover), not ground level. The deviations in E or N of check points calculated and averaged from four geocoded images are also shown in Figure 7 to understand the error behavior. Notice that Figure 5 and 7 demonstrate a similar trend of error curve. It means that the accuracy of the DEM generated and refined is comparable with that of the reference DEM in flat-moderate areas.

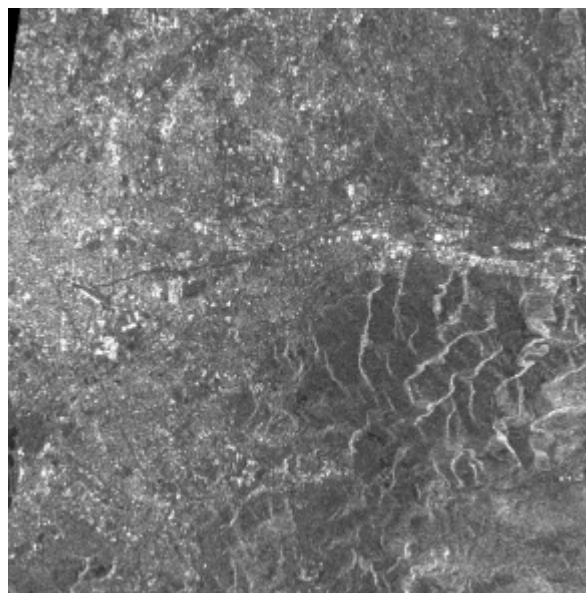


Figure 6. Geocoded image DS1 derived using the DEM generated and refined (Size: 11km × 11 km)

| Alias Name | DS1 | | DS7b | | AS1 | | AS7 | | Mean (m) | |
|------------|-----|----|------|----|-----|----|-----|----|----------|----|
| Component | E | N | E | N | E | N | E | N | E | N |
| Mean (m) | -16 | +7 | 0 | +5 | -10 | +7 | -7 | -4 | -8 | +4 |
| RMSE (m) | 15 | 10 | 14 | 24 | 20 | 13 | 20 | 20 | | |
| 2D (m) | 18 | | 28 | | 24 | | 28 | | | |

Table 5. Positioning accuracy of the check points measured in respect to each geocoded image derived using the generated DEM.

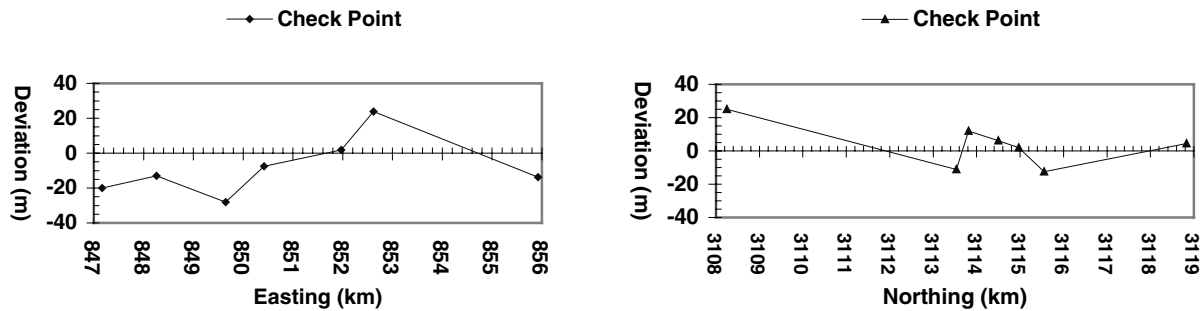


Figure 7. Deviations of the check points (in easting, above, and in northing, below) measured and averaged from the four geocoded images derived using the generated DEM.

In order to give a close look at the geocoded images, Figure 8 shows the image chips extracted from the geocoded images (DS1) derived using the generated DEM (left), those using the reference DEM (central) and the absolute difference image of both images (right). The darker the right image, the greater the difference in grey value. The size of each image chip in Figure 8 is 2.5km × 2.5km. The geocoded images in the top row are sectioned within a hilly area. The geocoded images in the bottom row are extracted from a flat-moderate area.

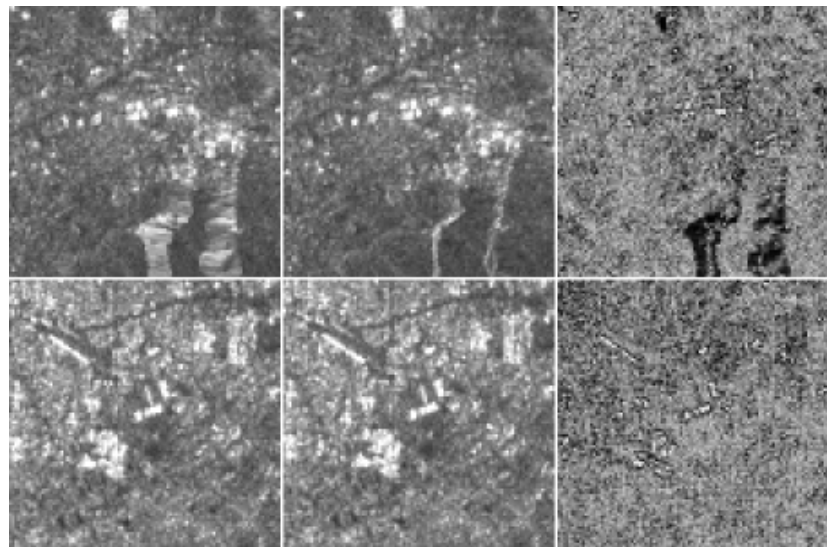


Figure 8. Geocoded image chips (DS1) in a hilly area (top row) and in a moderate-flat area (bottom row). (Left: the geocoded image using the reference DEM. Central: the geocoded image using the DEM derived. Right: the difference image of the left and the central images. Size: 2.5km × 2.5km. The darker the right image, the greater the difference in grey values.)

Obviously, the absolute difference image shows that image distortion in the hilly areas is evident (images in the upper row), but not in the moderate-flat areas. Notice that the roads (the dark lines) of the left and middle geocoded images in Figure 8 cannot be identified in the absolute difference image, i.e., the geometrically rectified locations of the roads in both images are overlapping each other (see the right images). Most of the bright objects (buildings) in the geocoded images of both rows are also overlapping each other, the high brightness spots showing correct geocoding. Particularly, the location of a train station in the images in the bottom row has been geometrically rectified correctly giving a bright linear feature. It proves that the quality of the generated DEM is suitable for geocoding in flat-moderate areas. However, the layover areas as shown at the bottom part of the geocoded images in the upper row cannot be rectified completely giving the dark areas as shown at the bottom of the upper-right image.

5 CONCLUSIONS

According to the results shown above, the rigidity and robustness of the proposed algorithms have been demonstrated. A higher level of automation for extracting spatial information and providing control is achieved and there is no manually selected GCPs required. The quality of the automatically generated GCPs assures that reliable ground control is provided. Geocoding employing the DEM generated using the stereo-SAR method is practical in moderate relief areas, provided that layover effects on SAR imagery are minimal.

ACKNOWLEDGMENTS

The authors are grateful to RADARSAT International (RSI) for providing the RADARSAT SAR images under the Application Development and Research Opportunity (ADRO) Programme. P.-H. Chen is grateful to the Government of the Republic of China and the Chung Cheng Institute of Technique for the full sponsorship of overseas Ph.D. study at University College London in U.K.

REFERENCES

- Chen, P.-H., 2000. *Extraction of Spatial Information from Stereoscopic SAR Images*. Ph.D. thesis submitted to University of London. 237 pages.
- Chen, P.-H. and Dowman, I. J., 1996. Space intersection from ERS-1 synthetic aperture radar images. *Photogrammetric Record*, 15 (88):561-573.
- Clark, C., 1991. *Geocoding and Stereoscopy of Synthetic Aperture Radar Images*. Ph.D. Thesis, University of London. 223 pages.
- CSA, 1995. *RADARSAT Canadian Data Processing Facility Product Specification*. Canadian Space Agency. CDRL No.IS-3, MacDonald-Dettwiler, Canada.
- Denos, M., 1992. A pyramidal scheme for stereo matching SIR-B imagery. *International Journal of Remote Sensing*, 13(2):387-392.
- Dowman, I.J. and Chen, P.-H., 1998. A rigorous stereo method for RADARSAT data. *RADARSAT ADRO Final Symposium*, Montreal. CD-ROM.
- Dowman, I.J, Laycock, J. and Whalley, J., 1993. Geocoding in the UK. In *SAR Geocoding: Data and Systems*. Edited by Schreier, G. Wichmann Verlag, Heidelberg, pp:373-387.
- Guindon, B., 1995. Performance evaluation of real-simulated image matching techniques in the acquisition of ground control for ERS-1 image geocoding. *ISPRS Journal of Photogrammetry and Remote Sensing*, 50(1): 2-11.
- JPL, 2000. *Shuttle Radar Topography Mission (SRTM)*. Jet Propulsion Laboratory. <http://www.jpl.nasa.gov/srtm> (17 March 2000).
- Kowk, R., Curlander, J.C. and Pang, S.S., 1990. An automated system for mosaicking spaceborne SAR imagery. *International Journal of Remote Sensing*, 11(2):209-223.
- Leberl, F.W., 1990. *Radargrammetric Image Processing*. Artech House Inc., Norwood, U.S.A. 595 pages.
- Otto, G.P. and Chau, T.K.W., 1989. Region-growing algorithm for matching of terrain images. *Image Vision Computing*, 7(2):83-94.
- Twu, Z.-G., 1996. *Automatic Height Extraction from Stereoscopic SAR Imagery*. Ph.D. Thesis, University of London. 222 pages.